Edinburgh Research Explorer

Linking [M-3(III)] triangles with "double-headed" phenolic oximes

OPEN ACCESS

Linking [M$^{III}_3$] triangles with "double-headed" phenolic oximes**

Kevin Mason,[1] John Chang,[1] Alessandro Prescimone,[1] Elena Garlatti,[2,3] Stefano Carretta,[3,]*

Peter. A. Tasker[1,]* and Euan K. Brechin[1,]*

[1]EaStCHEM, School of Chemistry, Joseph Black Building, University of Edinburgh, West Mains Road, Edinburgh, EH9 3JJ, UK.

[2]Dipartimento di Scienze Molecolari Applicate ai Biosistemi, Università di Milano, Via Trentacoste 2, 20134 Milano, Italy.

[3]Dipartimento di Fisica, Università di Parma, I-43124 Parma, Italy.

[*]Corresponding authors; S.C.: stefano.carretta@fis.unipr.it; P.A.T.: peter.tasker@ed.ac.uk, fax: +44-131-650-6453, tel: +44-131-650-7545; E.K.B.: e.brechin@ed.ac.uk

[**]Dedicated to Professor David Cole-Hamilton on the occasion of his retirement and for his outstanding contribution to transition metal catalysis.

Abstract

Strapping two salicylaldoxime units together with aliphatic α,Ω-aminomethyl links in the 3-position gives ligands which allow the assembly of the polynuclear complexes [Fe$_7$O$_2$(OH)$_6$(H$_2$L1)$_3$(py)$_6$](BF$_4$)$_5 \cdot$6H$_2$O$\cdot$14MeOH (**1**$\cdot$6H$_2$O$\cdot$14MeOH), [Fe$_6$O(OH)$_7$(H$_2$L2)$_3$][(BF$_4$)$_3$]$\cdot$4H$_2$O$\cdot$9MeOH (**2**$\cdot$4H$_2$O$\cdot$9MeOH) and [Mn$_6$O$_2$(OH)$_2$(H$_2$L1)$_3$(py)$_4$(MeCN)$_2$](BF$_4$)$_5$(NO$_3$)$\cdot$3MeCN$\cdot$H$_2$O$\cdot$5py (**3**$\cdot$3MeCN$\cdot$H$_2$O$\cdot$5py). In each case the metallic skeleton of the cluster is based on a trigonal prism in which two [M$^{III}_3$O] triangles are tethered together *via* three helically twisted double-headed oximes. The latter are present as H$_2$L^{2-} in which the oximic and phenolic O-atoms are deprotonated and the amino N-atoms protonated, with the oxime moieties bridging across the edges of the metal triangles. Both the identity of the metal ion and the length of the straps connecting the salicylaldoxime units have a major impact on the nuclearity and topology of the resultant cluster, with, perhaps counter-intuitively, the longer straps producing the "smallest" molecules.

Introduction

The development of crystal engineering and the synthesis of porous materials having metal organic frameworks (MOFs) has made extensive use of metal complexes as connecting nodes in lattices.[1] Transition metal complexes of salicylaldoximes have great potential as building blocks in supramolecular chemistry because they form two very stable types of platforms which are easily functionalized *via* the benzene rings (Figures 1 and 2).[2]

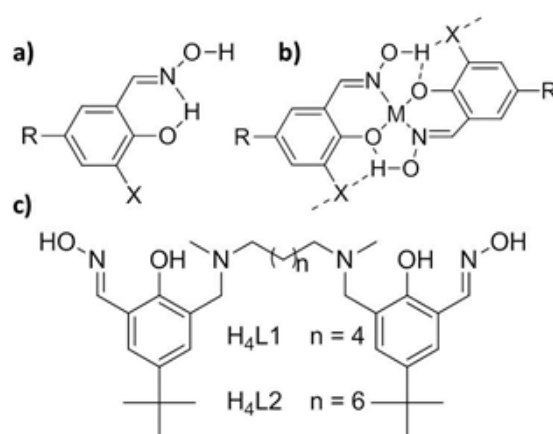**Figure 1.** (a) Structure of the phenolic oxime H$_2$L. (b) The planar mononuclear complexes [M(HL)$_2$] with 2-fold symmetry relating the X-substituents of the salicylaldoximate(-1) units. This structure is commonly observed for transition metals in the 2+ oxidation state. (c) Structure of the ligands H$_4$L1 (n = 4) and H$_4$L2 (n = 6).
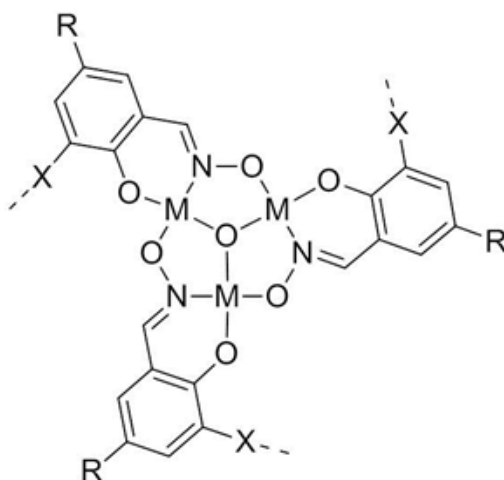
Figure 2. The planar trinuclear complexes [M^{III}$_3$O(L)$_3$]$^+$ of trivalent metal cations with 3-fold symmetry relating the X-substituents of the salicylaldoximate(-2) units.

The mononuclear planar complexes formed by mono-deprotonated forms of the ligands (Fig. 1b) have 2-fold symmetry[3] and are stabilized by inter-ligand hydrogen bonding which can be buttressed by incorporating electronegative substituents (X) *ortho* to the phenolic oxygen atom.[4] This *pseudo*-macrocyclic structure is responsible for the strength and selectivity of hydrocarbon-soluble versions (*e.g.* R = nonyl and X = H) as solvent extractants for copper and their success in commercial operations, which account for *ca.* 25% of worldwide production.[5] The planar trinuclear motif shown in Figure 2 is present in many μ$_3$-oxo-bridged complexes formed by doubly deprotonated salicylaldoximes.[6] These are most readily formed by trivalent transition metal ions, and often show unusual magnetic properties as a consequence of the proximity of the metal centres and coupling *via* the oximato- and oxo-bridging units.[6-8] The formation of other types of polynuclear iron structures leads to materials which contain iron(III) oxyhydroxide units resembling mineral structures with pigmentary properties and possibly accounts for the use of hydrophobic salicylaldoximes as corrosion inhibitors for iron.[9]

Strapping two salicylaldoxime units together in the 3-position, using ligands with aliphatic α,Ω-aminomethyl links (Fig. 1c) allows the assembly of polynuclear complexes which contain the stable motifs shown in Figures 1b and 2.[10] Copper(II) and nickel(II) form cages with *pseudo* 2-fold symmetry (Fig. 3a), which tightly and selectively bind anions (X) in the protonated cavities.[10a] This paper considers the formation of higher nuclearity complexes [of Fe(III) and Mn(III)] using the strapped ligands H$_4$L1 and H$_4$L2 (Fig. 1c). One of the features of interest is the extent to which the length and flexibility of the straps control the approach of triangular units to each other (*i.e.* the cavity size) and the how this in turn influences the ability of the molecule to accommodate anions and/or paramagnetic metal ions that can modify the magnetic exchange between triangles, as shown schematically in Fig. 3.
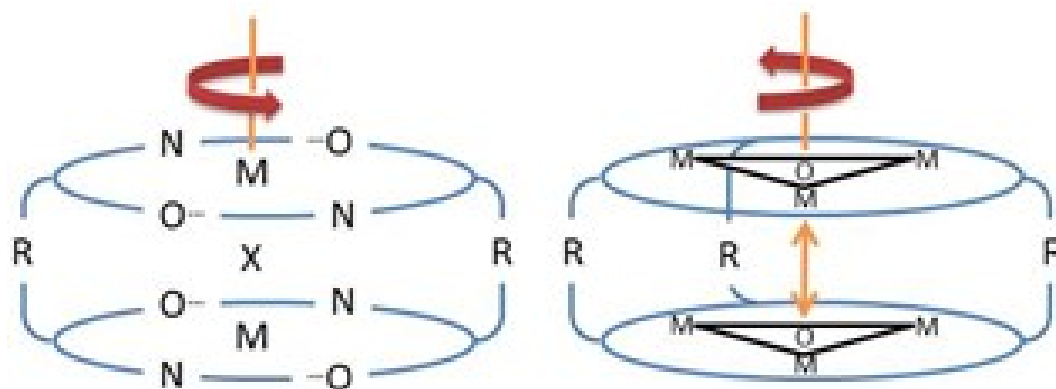
Figure 3. Cage structures with 2-fold symmetry (left) which encapsulate anions when the straps (R) are protonated α,Ω-aminomethylalkanes. Structures with 3-fold symmetry (right) in which the separation of the trinuclear metal units is related to the twist about the 3-fold axis allowed by the flexible α,Ω-diaminomethylalkane straps.

Experimental

Syntheses

All manipulations were performed under aerobic conditions using chemicals as received, unless otherwise stated.

H₄L1 [N,N'-dimethyl-N,N'-hexamethylenedi(3-hydroxyiminomehyl-2-hydroxy-5-*tert*-butylbenzylamine)] was prepared as described in the literature.[11]

H₄L2 [N,N'-dimethyl-N,N'-octamethylenedi(3-hydroxyiminomehyl-2-hydroxy-5-*tert*-butylbenzylamine]. To a mixture of potassium hydrogen carbonate (1.550 g, 15.5 mmol) and N,N'-dimethyl-1,8-octanediamine (0.946 g, 5.5 mmol) in acetonitrile (60 mL) was added an acetonitrile solution (60 mL) of 3-bromo-5-tertbutylsalicylaldehyde (3.186 g, 11.8 mmol) under nitrogen. The mixture was put under reflux for 16 hours to produce a yellow solution with a white precipitate. The precipitate was filtered and the filtrate concentrated on a rotary evaporator, before being loaded into a silica gel column and eluted with 50% ethyl acetate/n-hexane. The first yellow band was collected and reduced to dryness to give the dialdehyde precursor as an orange oil. The oil was dissolved in absolute ethanol (50 mL) to give a yellow solution, to which was added freshly generated hydroxylamine - prepared from hydroxylamine hydrochloride (0.941 g, 13.5 mmol) and potassium hydroxide (0.712 g, 12.7 mmol) in absolute ethanol (60 mL). The mixture was put under reflux for 6 hours and then filtered. The resulting white precipitate was filtered, washed with (i) water, (ii) ice-cold ethanol, (iii) diethyl ether and then dried under reduced pressure. Yield = 2.301 g, 71.8%. LRMS(FAB+): [M+H]⁺ calc. for $C_{34}H_{55}N_4O_4$ 583.42; found 583.30. NMR: ¹H NMR (DMSO- d₆,

500 MHz): δ 1.27 (m, 22H, C$\underline{\text{H}}_2$CH$_2$CH$_2$CH$_2$N, (C$\underline{\text{H}}_3$)$_3$C), 1.28 (m, 4H, CH$_2$C$\underline{\text{H}}_2$CH$_2$CH$_2$N), 1.51 (m, 4H, CH$_2$CH$_2$C$\underline{\text{H}}_2$CH$_2$N), 2.23 (s, 6H, C$\underline{\text{H}}_3$N), 2.44 (t, 4H, $^3J_{HH}$ = 7.3 Hz), 3.69 (s, 4H, NC$\underline{\text{H}}_2$Ar), 7.18, 7.50 (d, 4H, $^4J_{HH}$ = 2.4 Hz, Ar-$\underline{\text{H}}$), 8.32 (s, 2H, C$\underline{\text{H}}$NOH). ^{13}C NMR (DMSO- d$_6$, 125 MHz): δ 26.1, 26.4, 28.6 (($\underline{\text{C}}$H$_2$)$_3$CH$_2$N), 31.1 (($\underline{\text{C}}$H$_3$)$_3$C), 33.6 ((CH$_3$)$_3$$\underline{\text{C}}$), 40.8 ($\underline{\text{C}}H_3$N), 56.0 ((CH$_2$)$_3$$\underline{\text{C}}H_2$N), 59.1 (Ar$\underline{\text{C}}H_2$N), 117.6, 121.1, 122.8, 126.8, 140.6, 145.4 (Ar-$\underline{\text{C}}$), 153.5 ($\underline{\text{C}}$HNOH). CHN: calculated (found) for C$_{34}$H$_{54}$N$_4$O$_4$: C: 70.07 (69.57), H: 9.34 (9.09), N 9.61 (9.51).

[Fe$_7$O$_2$(OH)$_6$(H$_2$L1)$_3$(py)$_6$](BF$_4$)$_5$·6H$_2$O·14MeOH (1·6H$_2$O·14MeOH): Fe(BF$_4$)$_2$·6H$_2$O (338 mg, 1 mmol) and H$_4$L1 (277 mg, 0.5 mmol) were dissolved in MeOH (25 ml) and after 5 minutes stirring pyridine (2 ml) was added. The dark red solution was stirred for a further 180 minutes then filtered and left to evaporate slowly. X-ray quality crystals were produced after 3 days with an approximate yield of 30%. Elemental Analyses, calculated (found) for C$_{129}$H$_{198}$B$_5$F$_{20}$Fe$_7$N$_{18}$O$_{29}$ (1·6H$_2$O·3MeOH): C: 47.09 (46.64), H: 6.07 (5.59), N: 7.66 (7.88). BF$_4^-$ content: anion content was determined to be five BF$_4^-$ ions per cluster by performing ion exchange chromatography on a Dionex ICS-1100 chromatography system with data analysis by Chromeleon software package. All equipment and parts were supplied by Dionex. The system utilises 4.5 mM sodium carbonate/1.4 mM sodium hydrogen carbonate eluent and 4-mm IonPac AS-22 anion exchange column was chosen for the analysis. The column temperature was set at 30 °C, flow rate at 1.2 mL/min, and a sample size of 25 µL. Detection method was by suppressed conductivity with a 4-mm ASRS 300 suppressor. Chromeleon version 6.8.

[Fe$_6$O(OH)$_7$(H$_2$L2)$_3$](BF$_4$)$_3$·4H$_2$O·9MeOH (2·4H$_2$O·9MeOH): Fe(BF$_4$)$_2$·6H$_2$0 (338 mg, 1 mmol) and H$_4$L2 (291 mg, 0.5 mmol) were dissolved in MeOH (25 ml) and after 5 minutes stirring pyridine (2 ml) was added. The dark red solution was stirred for a further 180 minutes then filtered and left to evaporate slowly. X-ray quality crystals were produced after 3 days with an approximate yield of 30%. Elemental Analyses, calculated (found) for C$_{111}$H$_{207}$B$_3$F$_{12}$Fe$_6$N$_{12}$O$_{33}$ (2·6H$_2$O·3MeOH): C: 47.05 (46.96), H: 7.36 (6.97), N: 5.93 (6.31).

[Mn$_6$O$_2$(OH)$_2$(H$_2$L1)$_3$(py)$_4$(MeCN)$_2$(NO$_3$)](BF$_4$)$_5$·3MeCN·H$_2$O·5py (3·3MeCN·H$_2$O·5py): Mn(NO$_3$)$_2$·4H$_2$O (126 mg, 0.5 mmol), H$_4$L1 (139 mg, 0.25 mmol) and NaBF$_4$ (110 mg, 1 mmol) were dissolved in MeCN (25 ml). After full dissolution to a yellow/brown mixture, pyridine was added (2 ml) and the subsequent dark green solution stirred for 2 hours. The resulting solution was then diffused with Et$_2$O and X-ray quality crystals were produced after 4 days with an approximate yield of 25%. Elemental Analyses, calculated (found) for C$_{151}$H$_{208}$B$_5$F$_{20}$Mn$_6$N$_{27}$O$_{20}$ (3·3MeCN·H2O·5py) C: 52.04 (52.34), H: 6.02 (5.69), N: 10.85 (10.68).

Physical Measurements

Elemental analyses (C, H, N) were performed by the EaStCHEM microanalysis service. Variable temperature magnetic susceptibility measurements were made on powdered polycrystalline samples restrained in eicosane using a Quantum Design MPMS-XL SQUID magnetometer. Diamagnetic corrections were applied using Pascal's constants. Single crystal X-ray crystallography was performed using a Bruker Smart Apex CCD diffractometer equipped with an Oxford Cryosystems LT device, using Mo radiation. Data collection parameters and structure solution and refinement details are listed below. Full details can be found in the CIF files; CCDC 814873 (**1**), 863633 (**2**) and 863634 (**3**).

Crystal data for (**1**·$6H_2O$·14MeOH): $C_{140}H_{242}B_5F_{20}Fe_7N_{18}O_{40}$, M = 3642.50, Dark Red Rod, 0.15 _ 0.08 _ 0.06 mm, monoclinic, space group $P2_1/n$, a =16.9480(11), b = 32.864(2), c = 31.135(2) Å, β = 94.336(4)°, V=17291.7(20)Å^3, Z=4, Bruker Apex II CCD, Mo-Kα radiation, λ=0.71073Å, T=150(2)K, 2θmax=53.006°, 110344 reflections collected, 36222 unique (Rint = 0.106). Final GooF = 1.0984, R_1 =0.1166, wR2=0.1115, R indices based on 17942 reflections with I > 2σ(I) (refinement on F^2). The "SQUEEZE procedure[12] has been used to treat the solvent and the remaining BF_4^- anion region. 1142 e-/cell were found therefore 285 e-/cluster unit had to be assigned to solvent molecules as thirteen MeOH, one water (244 e-) plus one BF_4 (41 e$^-$).

Crystal data for (**2**·$4H_2O$·9MeOH): $C_{111}H_{207}B_3F_{12}Fe_6N_{12}O_{33}$, M = 2821.28, Black Block, 0.16 _ 0.25 _ 0.27 mm, trigonal, space group $R\bar{3}c$, a, b =26.5317(4), c = 101.306(2) Å, V=61758.3(19)Å^3, Z=18, SuperNova, Dual, Cu at zero, Atlas, Cu-Kα radiation, λ=1.5418Å, T=100(2)K, 2θmax=51.6473°, 115307 reflections collected, 7558 unique (Rint = 0.1257). Final GooF = 1.0511, R_1 =0.1468, wR2=0.1769, R indices based on 6609 reflections with I > 2σ(I) (refinement on F). The "SQUEEZE procedure[12] has been used to treat the solvent region. 2981 e-/cell were found therefore 165 e-/cluster unit had to be assigned to solvent molecules as nine MeOH (162 e$^-$).

Crystal data for (**3**·3MeCN·H2O·5py): $C_{151}H_{208}B_5F_{20}Mn_6N_{27}O_{20}$, M = 3485.07, Black Block, 0.09 _ 0.11 _ 0.11 mm, monoclinic, space group $P2_1/c$, a = 32.9404(6), b = 18.7090(3), c = 28.3771(5) Å, β= 111.947(2)°, V= 16220.9(6) Å^3, Z=4, SuperNova, Dual, Cu at zero, Atlas, Cu-Kα radiation, λ=1.5418Å, T=100(2)K, 2θmax= 73.724°, 94960 reflections collected, 31620 unique (Rint = 0.042). Final GooF = 1.0970, R_1 =0.1377, wR2=0.1548, R indices based on 19343 reflections with F>4σ(F) (refinement on F^2). The "SQUEEZE procedure[12] has been used to treat the solvent region. 859 e-/cell were found therefore 212 e-/cluster unit had to be assigned to solvent molecules as five pyridine molecules (210 e$^-$).

Results and Discussion

The new clusters **1-3** have the expected architectures shown in Fig 3b. Whilst they all contain two μ_3-oxo

trinuclear units linked by three ligand straps, there are significant differences in their dispositions. These differences, which are compared in the conclusions section, can be characterised by the parameters in Table 1: (i) the variations in the distance between the central μ_3-oxygen atoms, (ii) the extents to which the units are parallel to each other, (iii) the extents to which the two triangular units are twisted relative to one another and (iv) whether the cavities between them are large enough to accommodate an additional metal ion and additional ligands bridging this to the metals ions in the triangular faces.

	1	2	3	4
μ_3-O…μ_3-O distance (Å)	6.920	2.526	5.188	7.237
Angle between least square planes defined by the μ_3-OM$_3$ units (°)	2.8	0.3	34.7	3.4
Twist angles M-O…O-M defined by the phenolate oxygen atoms in strapped ligands	68.7 69.6 68.6	111.2[a] 114.1[a] 114.1[a]	95.7 103.1 97.2	59.2 59.1 59.3
Mean value	69.0	113.1	98.6	59.2

Table 1. Parameters defining the shapes of the clusters **1 – 4**. [a]The ligand straps in this cluster do not define the shortest Fe…Fe distances between atoms in the two triangular faces (see Fig 5) but instead span diagonals of the rectangular faces of the trigonal prism. The Fe-O…O-Fe twist angles associated with the *sides* of the rectangles linking the triangular face are 5.42, 7.62 and 7.62°.

The reaction of Fe(BF$_4$)$_2$·6H$_2$O and H$_4$L1 in a MeOH/py solvent mixture produces dark red/black crystals of complex **1** that are in the monoclinic space group *P2$_1$/n*. The metallic skeleton of the cation of **1** (Figure 4) describes a [Fe$^{III}_3$]$_2$ trigonal antiprism consisting of two [Fe$^{III}_3(\mu_3$-O)]$^{7+}$ triangles linked centrally through the presence of a [Fe(OH)$_6$]$^{3-}$ moiety (Fe$_{triangle}$-OH-Fe$_{central}$, 133.37-135.75°) and peripherally by three helically twisted phenolic oxime ligands. Each oxime moiety bridges in a η^1: η^1: η^2: μ-mode along the edges of the [Fe$_3(\mu_3$-O^{2-})]$^{7+}$ triangles (Fe-N-O-Fe, 2.57-20.68°) in a fashion entirely analogous to that previously seen for salicylaldoximate-bridged [Mn$^{III}_3$] and [Mn$^{III}_6$] clusters.[6] The "doubled-headed" oximes are present as H$_2$L^{2-} in which the oximic and phenolic O-atoms are deprotonated and the amino N-atoms protonated. The N-atoms H-bond to three H$_2$O molecules which fill the remaining available space within the central cavity of the cluster (N...O, 2.849-2.969 Å), with the latter further H-bonding to both the central OH$^-$ ions and the oximic O-atoms (2.770-2.891 Å). The helical twisting of the organic strap linking the two bridging head groups results in a staggered antiprismatic arrangement of the iron atoms, with the planes of the two [Fe$_3$O] triangles sitting approximately parallel to each other (Figure 4 and Table 1). The distance

between the two mean planes of the [Fe^{III}_3] triangles is approximately 6 Å and the distance between the [Fe^{III}_3] triangles and the central Fe^{III} ion is ~3 Å. The O^{2-} ions do not sit directly in the [Fe_3] triangular planes, but instead are displaced (0.352, 0.318 Å) out of the plane, pointing away from the centre of the molecule. The six axial coordination sites on the faces of the triangles are filled by pyridine solvent molecules, which complete the octahedral [O_4N_2] geometry at these Fe^{III} ions. The central iron atom has an approximately octahedral [O_6] donor set with Fe-O distances of 1.921± 0.014 Å and *trans* and *cis* O-Fe-O angles falling in the ranges 176.0(2) – 177.7(2) and 87.9(2) – 93.3(2)˚, respectively.

Charge balance is ensured by the presence of five BF_4^- ions per cluster. In the crystal the closest inter-cluster interactions occur between neighbouring H_2L1^{2-} ligands, with C…C distances of the order of ~4 Å.
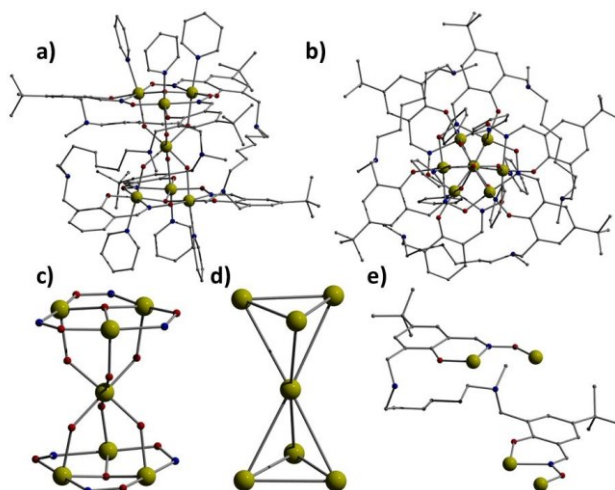

Figure 4. Molecular structure of the cation of **1** viewed parallel (a) and perpendicular (b) to the [Fe_3] planes. The magnetic core (c) and the metallic skeleton (d). (e) The coordination mode of H_2L1^{2-}. Colour code: Fe = yellow, O = red, N = blue, C = grey. H-atoms and anions omitted for clarity.

If the reaction that produced **1** is repeated, but employing H_4L2 instead of H_4L1 the related complex [$Fe_6O(OH)_7(H_2L2)_3$](BF_4)$_3$ (**2**) is formed (Figure 5). Interestingly the use of a longer, more flexible strap produces a smaller cluster in which the central cavity-filling Fe^{III} ion is no longer present. **2** crystallises in the trigonal space group *R-3c* with the metallic skeleton comprising a [Fe^{III}_3]$_2$ triangular prism. The two [Fe_3] triangles are not fully eclipsed, having Fe-O…O-Fe dihedral angles in the range ~5-8°. The two triangles are linked to each other *via* a total of six OH^- bridges (Fe-O-Fe, 102-104°), two on each vertex, and three helical H_2L2^{2-} ligands. The six OH^- ions form an internal hexagon with O…O distances of ~2.4 Å between atoms bridging the same two Fe atoms and ~2.7 Å between neighbouring pairs. The coordination mode of the phenolic oxime ligands are exactly the same as that seen for H_2L1^{2-} in complex **1** (Fe-N-O-Fe,

15.87-26.33), although the twisting of the strap between the triangles is somewhat different. This is best observed when viewing the complex perpendicular to the two triangular faces of the prism (Figure 5b). For **2** the atoms bridging across each edge in the "upper" triangle follow the clockwise sequence Fe-N-O-Fe. In the lower triangle the atom sequence is reversed, Fe-O-N-Fe. This contrasts to complex **1** in which the Fe-N-O-Fe clockwise sequence is observed for both triangles. Again the μ_3-O atoms at the centre of the [Fe$_3$] triangles are displaced from the [Fe$_3$] plane (0.317 Å), but this time they point inwards, toward the "empty" cavity between the two [Fe$_3$] triangles and the six OH$^-$ ions. The distance between these two O-atoms is just 2.526 Å, suggesting the presence of a shared proton and thus a [O…H…O]$^{3-}$ unit.

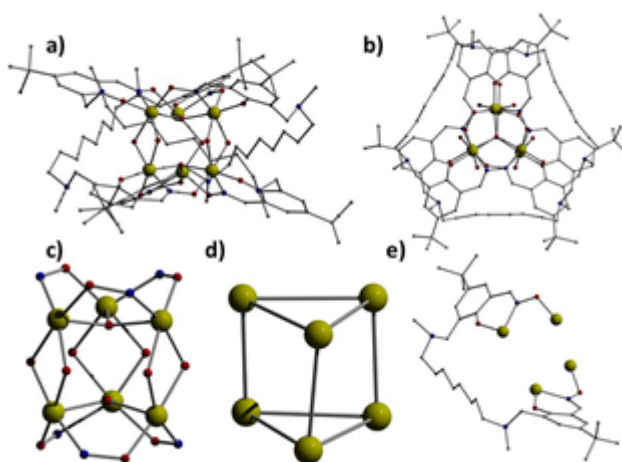**Figure 5.** Molecular structure of the cation of **2** viewed parallel (a) and perpendicular (b) to the [Fe$_3$] planes. The magnetic core (c), and the metallic skeleton (d). (e) The coordination mode of H$_2$L2^{2-}. Colour code as Fig. 4.

Indeed this is confirmed by BVS calculations which reveal a value of ~1.5 for each O-atom. The result is that the bridging -N-O- moieties from the H$_2$L2^{2-} ligands are now also displaced out of [the other side of] the [Fe$_3$] plane by approximately 1.3 Å, and there are no terminally coordinated pyridine ligands. This is in contrast to complex **1** in which the -N-O- moieties and [Fe$_3$] triangles are co-planar.

Each Fe^{III} ion thus has a [O$_5$N] donor set and lies in distorted octahedral geometry. The N-atoms in the straps are again protonated and each H-bond to a phenolic O-atom (O…O, ~3 Å) and to a water molecule of crystallisation (N…O, 2.749 – 2.848 Å) that lies in the bowl-shaped cavities formed from the puckered phenolic oxime head groups. The latter also H-bond to both the oximic and phenolic O-atoms (O…O, ~2.56 – 2.98 Å). The distance between the two [Fe$_3$] mean planes is ~3 Å. Charge balance is maintained by the presence of three BF$_4^-$ ions per cluster. There are numerous close contacts between adjacent cluster cations, with the closest intermolecular interactions between N- and C-atoms on neighbouring H$_2$L2^{2-}

ligands (~3.6 – 3.9 Å). The cluster cations pack in layers down the *c*-axis, with each [Fe$_6$] cluster forming a [Fe$_6$]$_3$ wheel with its two neighbouring clusters in the *ab*-plane. The BF$_4^-$ anions reside both within the cavity formed at the centre of this wheel and in the planes between the layers of clusters. The result is the formation of an aesthetically pleasing honeycomb-like framework when viewed down the *c*-axis (Figure 6).
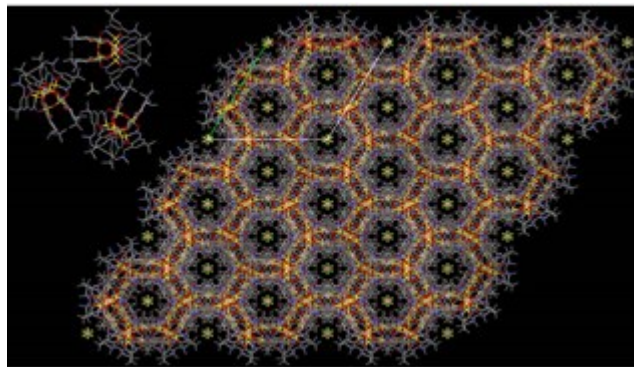

Figure 6. The packing of **2** in the crystal viewed down the *c*-axis. The inset (top left) shows the triangular wheel motif the cluster cations form with their two nearest neighbour clusters.

The reaction of Mn(NO$_3$)$_2$·4H$_2$O, H$_4$L1 and NaBF$_4$ in MeCN produces green/black crystals crystals of [Mn$^{III}_6$O$_2$(OH)$_2$(H$_2$L)$_3$(py)$_4$(MeCN)$_2$(NO$_3$)](BF$_4$)$_5$·3MeCN·H$_2$O·5py (**3**·3MeCN·H$_2$O·5py) that are in the monoclinic space group *P2/c*. The metallic skeleton of the cationic cluster describes a very distorted trigonal prism, with the molecule perhaps better described as possessing a clam-shell like structure (Figure 7) consisting of two [Mn$_3$O]$^{7+}$ triangles linked to each other through two hinge-like OH$^-$ ions (Mn-O-Mn, 141.39º, 145.54º; Mn-O, 2.158-2.315 Å) and three helical H$_2$L1^{2-} ligands. Each phenolic oxime moiety bridges in a η^1: η^1: η^2: μ-mode along the edges of the [Mn$^{III}_3$(μ$_3$-O^{2-})]$^{7+}$ triangles, in a manner identical to that observed for **1** and **2**. The planes of the two [Mn$_3$O] triangles sit at an angle of ~34.5º with respect to each other (Figure 7), with the metal atoms twisted [Mn-O…O-Mn] by approximately ~21° away from a trigonal prismatic arrangement – as can be seen when viewing the molecule perpendicular to the [Mn$_3$O] planes.

As for complex **2**, the atoms bridging across each edge in the "upper" triangle follow the clockwise sequence Mn-N-O-Mn, with the sequence reversed, Mn-O-N-Mn in the "lower" triangle. The O^{2-} ions are displaced out of the [Mn$_3$] plane (0.219, 0.224 Å). The "upper" and "lower" coordination sites on the triangular faces pointing away from the central cavity are occupied by a combination of terminally bonded py (x4) and MeCN (x2) molecules.
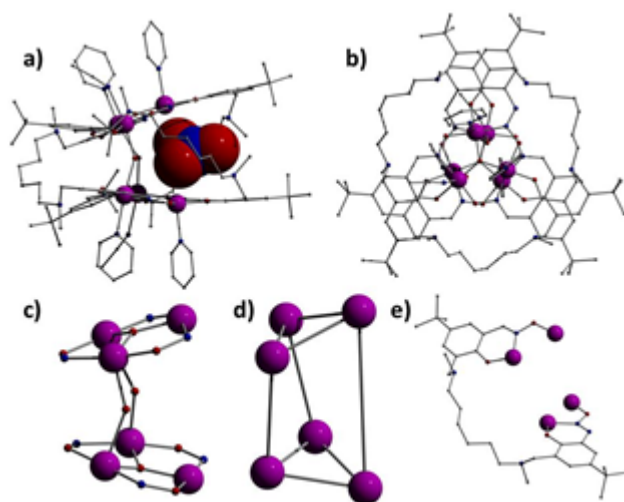
Figure 7. Molecular structure of the cation of **3** viewed parallel (a) and perpendicular (b) to the [Mn₃] planes. The magnetic core (c), and the metallic skeleton (d). (e) The coordination mode of H_2L1^{2-}. Colour code as Fig. 1. Mn = purple.

The four Mn ions at the hinge of the clamshell are six-coordinate and in distorted octahedral geometries with the Jahn-Teller axes defined by the N(solvent)-Mn-OH(hinge) vector. The two Mn ions at the open end of the clamshell are five-coordinate and square-based pyramidal in geometry with four short equatorial bonds and one long axial bond to the N-atom of a py molecule (Mn…N, 2.188, 2.252 Å). The vacant "inner" coordination sites result in the presence of a cavity between the planes that has an approximate volume of ~60 Å³ and which is occupied by a single NO_3^- anion. A space-filling representation (Figure 7a) clearly shows this to be a good fit to the cavity size. The O-atoms of the NO_3^- anion are H-bonded to the OH⁻ hinges (O…O, ~2.75 Å) and to the protonated amino N-atom of the organic strap (O…N, ~2.96 Å), with the latter also H-bonded to the terminally bonded phenolic O-atoms (~2.78 Å). They are also in close proximity to the phenolic and oximic O-atoms of the H_2L^{2-} ligands (O…O, ~2.85 Å) above and below. The inter-triangular metal-metal distances measure ~4.2 Å across the hinge and ~5.9 Å across the open face of the clam-shell. Charge balance is maintained by the presence of five BF_4^- anions per cluster. In the crystal the closest inter-cluster interactions occur between neighbouring H_2L1^{2-} ligands, with C…C distances of the order of ~4 Å, and *via* π…π stacking of adjacent py molecules. The clusters pack in regular sheets in the *ac* plane with the anions filling the spaces between these sheets.

Intriguing questions arise from the formation of complex **3**. Why does the cluster form in a "squashed" clamshell topology in which the [Mn$^{III}_3$] triangles are relatively closely spaced and in which the organic straps are not "fully" extended? Why is a NO_3^- anion incorporated in the cavity when the "pocket" appears to be ideally sized for the introduction of a seventh metal(III) ion, as is the case in the Fe₇ system, **1**, especially since the cluster requires the presence of *six* counter anions for charge balance? It is possible

that a Jahn-Teller distorted Mn(III) ion will not sit comfortably within an octahedral cavity of the type observed in **1** (see above) created by two antiprismatic [Mn$_3$O] triangles and it was more likely that a Mn(II) ion could taken up. We have previously shown that triangular face-capping Mn(II) ions can easily be incorporated onto oxime-based [Mn$^{III}_3$] triangles through the addition of N$_3^-$,[13] and indeed repetition of the reaction that produces **3** but in the presence of NaN$_3$ rather than NaBF$_4$ produces triclinic green/black crystals that contain the complex [Mn$^{III}_6$Mn$^{II}_2$O$_2$(N$_3$)$_6$(H$_2$L)$_3$(MeCN)$_6$]$^{4+}$ (**4**). Unfortunately the X-ray data do not permit the identification of any counter ions and/or solvent molecules as the diffraction quality decreases very sharply above 1.0 Å of resolution. This is a clear indication of a very disordered structure, although the connectivity of the cationic cluster (Figure 8) could be clearly established and even the conformational disorder of one of the oximic ligands could be modelled. Repetition of the synthesis of the complex has proven difficult, resulting in an inability to isolate, purify and analyse by other methods. Consequently we include only a brief description of the structure of the cation of **4**. This Mn$_7$ cluster (Figure 8), like the Fe$_7$ system **1,** has a trigonal antiprismatic arrangement of the two [M$^{III}_3$O]$^{7+}$ triangles which are linked to each other through three greatly extended helical H$_2$L1^{2-} ligands. The columnar cavity is occupied by a single Mn(II) ion, linked to the upper and lower [Mn$^{III}_3$] triangles by six (end-on) μ-bridging N$_3^-$ ions (Mn^{III}-N-Mn^{II}, ~121-131°). The coordination mode of the phenolic oxime ligands (Fig 8e) is the same as that seen in complex **1** in which the bridging ligands define twist angles of 59° between the triangular faces of the antiprism.
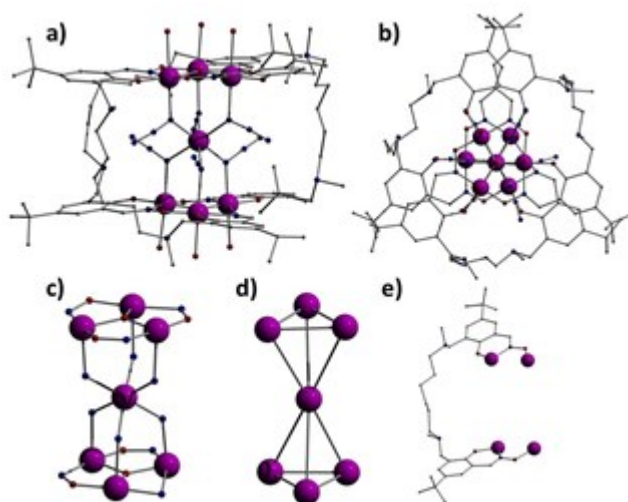
Figure 8. Molecular structure of the cation **4** viewed parallel (a) and perpendicular (b) to the [Fe$_3$] planes. The magnetic core (c), and the metallic skeleton (d). (e) The coordination mode of H$_2$L1^{2-}.

The distance between the two mean planes of the co-planar [Mn$^{III}_3$] triangles of the upper and lower faces of the prism is ~7 Å. All manganese ions have distorted octahedral geometries with the coordination sites

on the faces of the [Mn$_3$] triangles completed by terminally bonded solvent molecules. The central Mn(II) ion has a [N$_6$] coordination sphere with Mn-N distances of 2.137 ± 0.051 Å and *trans* and *cis* N-Mn-N angles falling in the ranges 177.31 – 179.49 and 87.33 – 92.92° respectively. The Mn(III) ions have [O$_4$N$_2$] donor sets with their Jahn-Teller extended axes perpendicular to the [Mn$_3$] triangles (N(azide)-Mn-O(solvent)).

Magnetic Measurements

The magnetic properties of **1**, **2** and **3** have been investigated by measuring the temperature-dependence of their magnetic susceptibilities (Figures 9-11). All the compounds are characterised by a monotonic decrease of χT down to low temperatures, suggesting the presence of sizeable antiferromagnetic (AF) interactions. Indeed this is also reflected in the fact that the room-temperature values of χT are significantly smaller than that corresponding to non-interacting ions, especially in **1** and **2.**

As a first approximation, the magnetic properties of **1**, **2** and **3** can be modelled by the isotropic Heisenberg spin Hamiltonian:

$$H = \sum_{i>j} J_{ij} S_i \cdot S_j + g\,\mu_B B \cdot \sum_i S_i \qquad (1)$$

($S_i = 5/2$ for Fe^{3+} and $S_i = 2$ for Mn^{3+}). The last term accounts for the Zeeman interaction with the applied magnetic field **B**. The patterns of exchange constants are illustrated in the insets of Figures 9-11. Given that Fe^{3+} is characterised by a half-filled *d*-electron shell, anisotropic exchange and crystal-field interactions in **1** and **2** are expected to be small and (1) should provide a very good description of these molecules. Conversely, further anisotropic terms could be important in **3**, especially to describe the low-temperature behaviour. In the Zeeman term we have assumed $g = 2$, consistent with the typical behaviour of Fe^{3+} (for **1** and **2**) and with the values observed in a family of structurally related Mn$^{III}_6$ compounds (for **3**).[14]

The simplest conceivable models of these molecules are characterised by two exchange constants only, one describing intra-triangle exchange coupling and one describing the other bonds (see insets in Figures 9-11). However, these models are not adequate to describe the observed magnetic behaviour. Indeed, the structures of **1**, **2** and **3** allow for *several* distinct exchange parameters. In the following we therefore describe the simplest models that allow for a satisfactory fit of the temperature-dependence of magnetic susceptibility.
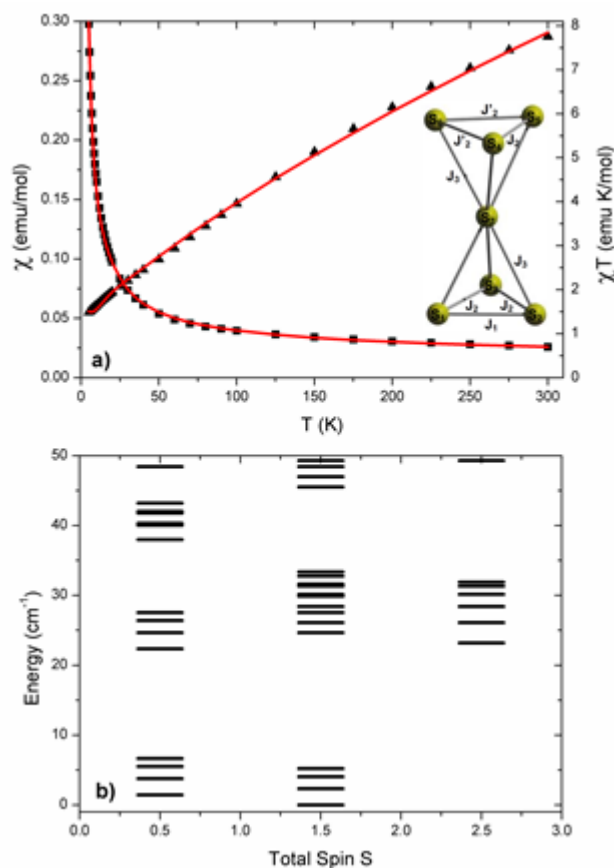
Figure 9. a) Measured temperature dependence of the magnetic susceptibility of **1** (black squares), also reported as χT (black triangles). Red lines represent calculations with $J_1 = 58$ cm^{-1}, $J_2 = 63.2$ cm^{-1}, $J'_2 = 63.8$ cm^{-1}, $J_3 = 53.3$ cm^{-1} and $g = 2$. Inset: schematic representation of the seven Fe^{3+} ions and of the exchange couplings. b) Exchange energy of the lowest total spin multiplets calculated with the spin Hamiltonian (1) and the above exchange constants. The ground state energy is set to zero.

The low-T value of χT in **1** points to a low total-spin S ground state and to the presence of low-lying excited states (the measured value is smaller than that corresponding to an isolated $S = 3/2$ multiplet). Figure 9 shows that magnetic measurements can be well reproduced by a model characterised by strong AF exchange couplings both within the upper and lower Fe triangles and between these triangles and the central Fe ion.

The presence of these competing interactions leads to a low-spin ground multiplet and to several low-lying excited manifolds (Figure 9 b).

The fitting of the magnetic data of **1** within the present model is *not* unique and the parameters are correlated; indeed the data can be acceptably reproduced by several regions of the parameter space (see the Supplementary Information for further details). For instance, a very good agreement with the data is

obtained with $J_1 = 58$ cm^{-1}, $J_2 = 63.2$ cm^{-1}, $J'_2 = 63.8$ cm^{-1}, $J_3 = 53.3$ cm^{-1}. For this particular family of parameters the order of magnitude of the Fe-Fe superexchange couplings are consistent with the model introduced by Cañada-Vilalta et al.[15] to explain magneto-structural correlations in molecular clusters containing Fe^{3+} ions.

The low-temperature value of χT in **2** suggests a non-magnetic $S = 0$ ground state very close to a magnetic $S = 1$ triplet. The observed magnetic behaviour of **2** is reproduced by assuming strong AF coupling within the two triangles and weak inter-triangle interactions (see Figure 10). Best fits are obtained with a unique set of parameters: $J_1 = (43 \pm 4)$ cm^{-1}, $J_2 = (56 \pm 5)$ cm^{-1}, $J_3 = (0.6 \pm 0.05)$ cm^{-1}. The order of magnitude of intra-triangle exchange couplings are again in agreement with the Cañada-Vilalta model.[15] The inter-triangle interaction is small, but consistent with other clusters with similar Fe-Fe super-exchange bridges.[16,17] Hence, this system is also characterised by the presence of competing interactions. The presence of strong AF interactions in both **1** and **2** explains the large room-temperature reduction of the effective moment in these compounds with respect to that of uncoupled ions. Figure 10b shows that the present model is characterised by a singlet ground state and by an excited triplet well separated from the other excited levels.

← **Figure 10.** a) Measured temperature dependence of the magnetic susceptibility of **2** (black squares), also reported as χT (black triangles). Red lines are obtained with $J_1 = 43$ cm^{-1}, $J_2 = 56$ cm^{-1}, $J_3 = 0.6$ cm^{-1} and $g = 2$. Inset: schematic representation of the six Fe^{3+} ions and of the exchange couplings. b) Exchange energy of the lowest total spin multiplets calculated with the spin Hamiltonian (1) and the exchange constants reported above. The ground state energy is set to zero.
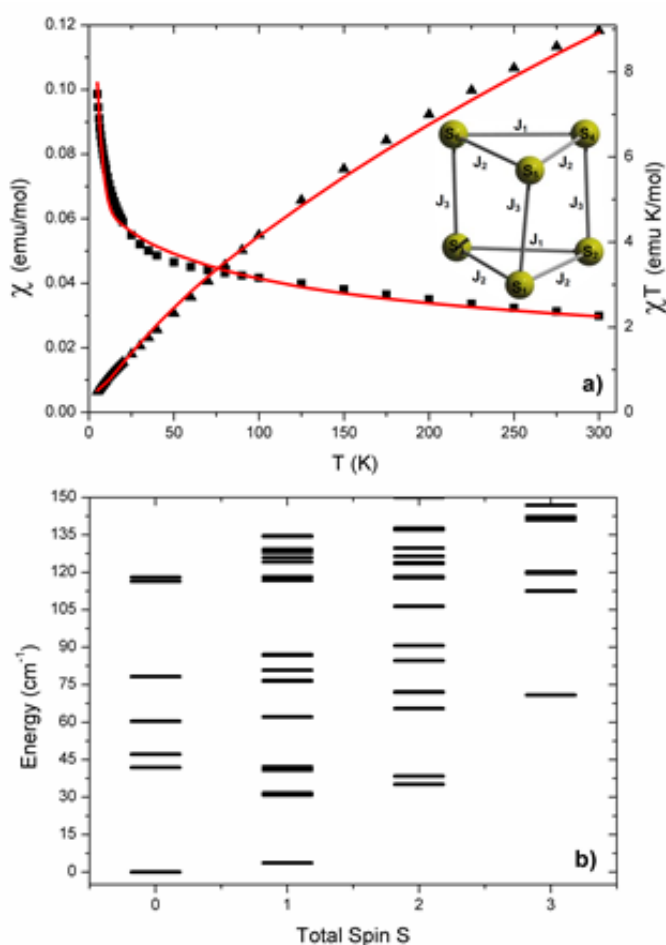
The temperature-dependence of the magnetic susceptibility of **3** can be reproduced with Eq (1) with a unique set of parameters, as shown in Figure 11a. The model is characterised by sizeable AF exchange interactions within the two Mn triangles, $J_1 = 18$ (± 2) cm^{-1}, $J_2 = 13$ (± 2) cm^{-1}, and by vanishing coupling between the triangles. The use of g-values other than 2 does not improve the fit. The resulting energy of the lowest-lying multiplets is reported in Figure 11b as a function of their total spin. The presence of low-lying magnetic states is necessary to account for the measured low-temperature susceptibility. As stated above, sizeable anisotropic interactions can be expected in **3,** but single-crystal measurements are needed to address this issue.
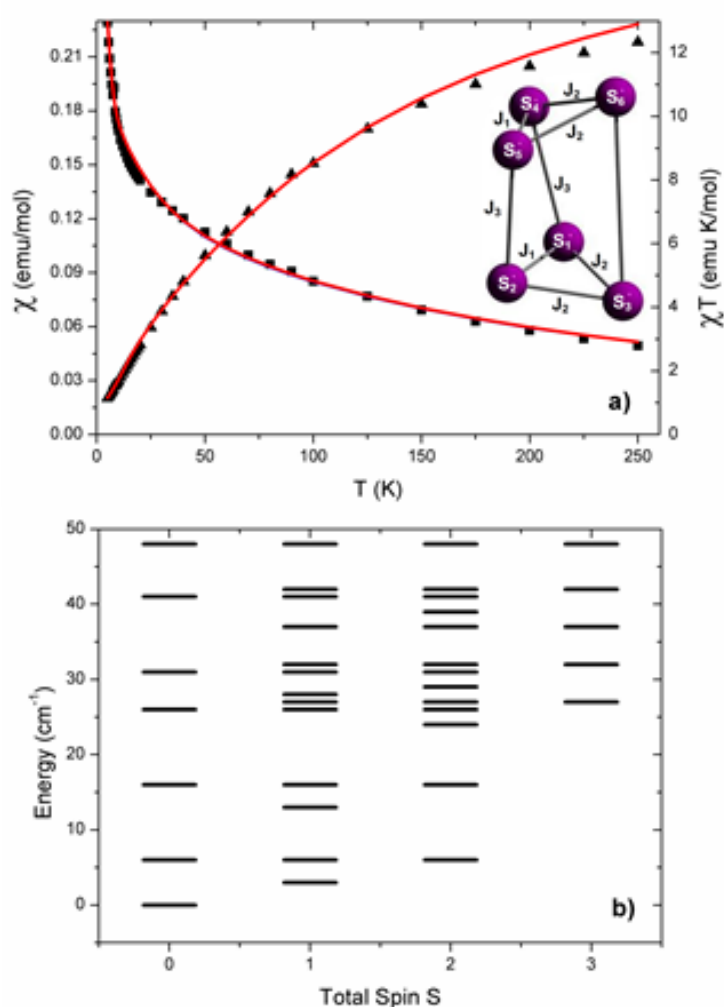
Figure 11. a) Measured temperature dependence of the magnetic susceptibility of **3** (black squares), also reported as χT (black triangles). Red lines are calculated with $J_1 = 18$ cm^{-1}, $J_2 = 13$ cm^{-1}, $J_3 = 0$ cm^{-1}. Inset: schematic representation of the six Mn^{3+} ions and of the exchange couplings. b) Exchange energy of the lowest total spin multiplets calculated with the spin Hamiltonian (1) and the above exchange constants. The ground state energy is set to zero.

Conclusions

The extent to which the structures of the clusters are controlled by the requirements of the strapped ligands, the metal ions' best use of bridging anions and the optimisation of forms of secondary bonding inside and outside the cavities containing the clusters can be compared using Table 1. The largest μ_3-O… μ_3-O separations are found in the Fe_7 and Mn_7 clusters, **1** and **4**, (6.920 and 7.237 Å). These allow the cavities defined by the triangular faces and the three aliphatic straps to accommodate $Fe(OH)_6^{3-}$ and $Mn(N_3)_6^{4-}$ units. These octahedral, central bridging units transmit an approximately 60° twist to the two triangular μ_3-OM_3 units, resulting in an anti-prismatic arrangement with mean twist angles of 69° and 59°. The shortest μ_3-O… μ_3-O distance, 2.526 Å, is present in the Fe_6 cluster, **2**. This allows each iron atom in one triangular face to form two μ_2-OH bridges to an iron atom in the other triangular face (see Fig 5), and results in the two triangular μ_3-OFe_3 units forming a prismatic arrangement. Unlike the other clusters which contain H_2L1^{2-}, the longer straps of H_2L2^{2-} do not define the shortest Fe…Fe distances between atoms in the two triangular faces (see Fig 5). They span a rectangular face of the trigonal prism in such a way that the Fe-O…O-Fe twist angles defined by the phenolate oxygen atoms of strapped ligands approach 120°.

The Mn_6 cluster, **3**, is the least regular, principally because the two triangular μ_3-OMn_3 units are not parallel. Their least squares planes are inclined at ~34.5°. Two Mn atoms in each triangular unit closely approach Mn atoms in the adjacent unit to form μ_2-OH bridges. The remaining Mn atoms in each triangle are more widely separated, accommodating a non-coordinated nitrate moleculae between them. It seems likely that this arrangement better suits the Jahn-Teller distorted Mn(III) atoms than the formation of a more compacted trigonal prism with six bridging hydroxides between the two triangular faces (as in the Fe^{III}_6 cluster, **2**) or of an extended trigonal antiprism with a bridging $Mn^{III}(OH)_6^{3-}$ unit between the two triangular faces (as in the Fe^{III}_7 cluster, **1**).

It is clear that the very flexible straps in the double headed phenolic oximes, H_4L1 and H_4L2, allow deprotonated forms to provide a range of clusters which can be represented by the schematic structure shown in Fig 1c. Their flexibility appears to ensure that the clusters which are isolated meet the electronic requirements of the M(III) ions which are present in the key μ_3-OM_3 building blocks which define their pseudo C_3 symmetry.

Notes and references

[1] See for example: (a) B. Moulton and M. J. Zaworotko, *Chem. Rev.*, 2001, **101**, 1629. (b) S. Kitagawa, R. Kitaura and S.-I. Noro, *Angew. Chem. Int. Ed.*, 2004, **43**, 2334. (c) M. Eddaoudi, D. B. Moler, H. Li, B. Chen, T. M. Reineke, M. O'Keefe and O. M. Yaghi, *Acc. Chem. Res.*, 2001, **34**, 319. (d) D. Bradshaw, J. B. Claridge, E. J. Cussen, T. J. Prior and M. J. Rosseinsky, *Acc. Chem. Res.*, 2005, **38**, 273. (e) X. Lin, J. Jia, P. Hubberstey, M. Schröder and N. R. Champness, *CrystEngComm.*, 2007, **9**, 438. (f) A. K. Cheetham, C. N. R. Rao and R. K. Feller, *Chem. Commun.*, 2006, 4780. (g) J. J. Perry IV, J. A. Perman and M. J. Zaworotko, *Chem. Soc. Rev.*, 2009, **38**, 1400. (h) D. J. Tranchemontagne, Z. Ni, M. O'Keefe and O. M. Yaghi, *Angew. Chem. Int. Ed.*, 2008, **47**, 5136.

[2] P. A. Tasker, P. G. Plieger and L. C. West, *Comprehensive Coordination Chemistry II,* 2004, **9**, 759.

[3] A. G. Smith, P. A. Tasker, *Coord. Chem. Rev.*, 2003, **241**, 61.

[4] R. S. Forgan, B. D. Roach, P. A. Wood, F. J. White, J. Campbell, D. K. Henderson, E. Kamenetzky, F. E. McAllister, S. Parsons, E. Pidcock, P. Richardson, R. M. Swart and P. A. Tasker, *Inorg. Chem.*, 2011, **50**, 4515.

[5] (a) P. J. Mackey, *CIM Magazine*, 2007, **2**, 35. (b) G. A. Kordosky, *Proceedings of the International Solvent Extraction Conference*, 2002, 853.

[6] See for example: (a) R. Inglis, C. J. Milios, L. F. Jones, S. Piligkos and E. K. Brechin, *Chem Commun.*, 2012, **48**, 181. (b) R. Inglis, S. M. Taylor, L. F. Jones, G. S. Papaefstathiou, S. P. Perlepes, S. Datta, S. Hill, W. Wernsdorefer and E. K. Brechin, *Dalton Trans.*, 2009, 9157. (c) R. Inglis, L. F. Jones, C. J. Milios, S. Datta, A. Collins, S. Parsons, W. Wernsdorfer, S. Hill, S. P. Perlepes, S. Piligkos and E. K. Brechin, *Dalton Trans.*, 2009, 3403. (d) C. J. Milios, S Piligkos and E. K. Brechin, *Dalton Trans.*, 2008, 1809.

[7] (a) K. Mason, I. A. Gass, S. Parsons, A. Collins, F. J. White, A. M. Z. Slawin, E. K. Brechin and P. A. Tasker, *Dalton Trans.*, 2010, **39**, 2727. (b) K. Mason, I. A. Gass, F. J. White, G. S. Papaefstathiou, E. K. Brechin and P. A. Tasker, *Dalton Trans.*, 2011, **40**, 2875. (c) I. A. Gass, C. J. Milios, A. Collins, F. J. White, L. Budd, S. Parsons, M. Murrie, S. P. Perlepes and E. K. Brechin, *Dalton Trans.*, 2008, 2043. (d) I. A. Gass, C. J. Milios, A. G. Whittaker, F. P. A. Fabbiani, S. Parsons, M. Murrie, S. P. Perlepes and E. K. Brechin, *Inorg. Chem.*, 2006, 45, 5281.

[8] (a) P. Chaudhuri, M. Hess, E. Rentschler, T. Weyhermüller and U. Florke, *New J. Chem.*, 1998, **22**, 553. (b) P. Chaudhuri, F. Birkelbach, M. Winter, V. Staemmler, P. Fleischhauer, W. Haase, U. Flörke and H.-J. Haupt, *J. Chem. Soc., Dalton Trans.*, 1994, 2313. (c) P. Chaudhuri, M. Winter, P. Fleischhauer, W. Haase, U. Flörke and H.-J. Haupt, *J. Chem. Soc., Chem. Commun.*, 1993, 566.

[9] (a) J. M. Thorpe, R. L. Beddoes, D. Collison, C. D. Garner, M. Helliwell, J. M. Holmes and P. A. Tasker, *Angew. Chem. Int. Ed.*, 1999, **38**, 1119. (b) A. K. Powell, S. L. Heath, D. Gatteschi, L. Pardi, R. Sessoli, G. Spina, F. Del Giallo and F. Pieralli, *J. Am. Chem. Soc.*, 1995, **117**, 2491. (c) G. W. Powell, H. N. Lancashire, E. K. Brechin, D. Collison, S. L. Heath, T . Mallah and W. Wernsdorfer, *Angew. Chem. Int. Ed.*, 2004, **43**, 5772.

[10] (a) M. Wenzel, G. B. Jameson, L. A. Ferguson, Q. W. Knapp, R. S. Forgan, F. J. White, S. Parsons, P. A. Tasker and P. G. Plieger, *Chem. Commun.*, 2009, 3606. (b) M. Wenzel, R. S. Forgan, A. Faure, K. Mason, P. A. Tasker, S. Piligkos, E. K. Brechin and P. G. Plieger, *Eur. J. Inorg. Chem.*, 2009, 4613.

[11] P. G. Plieger, P. A. Tasker and S. G. Galbraith, *Dalton Trans.*, 2004, 313.

[12] P. Van der Sluis and A. L. Spek, *Acta Crystallographica*, 1990, **A46**, 194.

[13] C. J. Milios, R. Inglis, L. F. Jones, A. Prescimone, S. Parsons, W. Wernsdorfer and E. K. Brechin, *Dalton Trans.*, 2009, 2812.

[14] C. J. Milios, R. Inglis, R. Bagai, W. Wernsdorfer, A. Collins, S. Moggach, S. Parsons, S. P. Perlepes, G. Christou and E. K. Brechin, *Chem. Commun.*, 2007, 3476.

[15] (a) C. Cañada-Vilalta, T. A. O'Brien, E. K. Brechin, M. Pink, E. R. Davidson and G.Christou, *Inorg. Chem.,* 2004, **43**, 5505. For other papers on magneto-structural correlations in Fe(III) chemistry, see for example: (b) H. Weihe and H. Güdel, *J. Am. Chem. Soc.*, 1997, **119**, 6539. (c) S. M. Gorun and S. Lippard, *Inorg. Chem.*, 1991, **30**, 1625.

[16] S. M. Gorun, G. C. Papefthymiou, R. B. Frankel and S. J. Lippard*, J. Am. Chem. Soc.*, 1987, **109**, 3337.

[17] D. M. Kurtz, *Chem. Rev.*, 1990, **90**, 585.

[18]